CHINESE OPTICS LETTERS

Vol. 21, No. 7 | July 2023

A detail-enhanced sampling strategy in Hadamard single-pixel imaging

Yan Cai (蔡 妍)[1], Shijian Li (李世剑)[1], Wei Zhang (张 伟)[1], Hao Wu (吴 昊)[1], Xuri Yao (姚旭日)[1,2*], and Qing Zhao (赵 清)[1,2**]

[1] Center for Quantum Technology Research and Key Laboratory of Advanced Optoelectronic Quantum Architecture and Measurements (MOE), School of Physics, Beijing Institute of Technology, Beijing 100081, China

[2] Beijing Academy of Quantum Information Sciences, Beijing 100193, China

*Corresponding author: yaoxuri@bit.edu.cn

**Corresponding author: qzhaoyuping@bit.edu.cn

Received January 7, 2023 | Accepted April 13, 2023 | Posted Online July 24, 2023

Hadamard single-pixel imaging is an appealing imaging technique due to its features of low hardware complexity and industrial cost. To improve imaging efficiency, many studies have focused on sorting Hadamard patterns to obtain reliable reconstructed images with very few samples. In this study, we propose an efficient Hadamard basis sampling strategy that employs an exponential probability function to sample Hadamard patterns in a direction with high energy concentration of the Hadamard spectrum. We used the compressed-sensing algorithm for image reconstruction. The simulation and experimental results show that this sampling strategy can reconstruct object reliably and preserves the edge and details of images.

Keywords: single-pixel imaging; compressed sensing; Hadamard matrix.

DOI: 10.3788/COL202321.071101

1. Introduction

Single-pixel imaging (SPI)[1] is one of the most representative applications of compressed-sensing (CS) theory[2,3] in imaging. An SPI system uses a spatial light modulator to illuminate an object with structured light or to modulate the light carrying the object information. A single-pixel detector is used to collect the partially sampled information light, which is then input into a reconstruction algorithm to recover an accurate image.

In SPI, the illumination pattern is a factor affecting the performance of the imaging system. SPI with a Hadamard basis has attracted much attention due to its advantages of simple generation and convenient application. Several studies have recently been conducted on Hadamard basis ordering. Cai *et al.*[4] proposed Hadamard pattern order based on Walsh codes to optimize its performance. Sun *et al.*[5] deeply investigated the Hadamard iteration law and proposed a new arrangement called the Russian Doll (RD order). Yu *et al.*[6] used the concept of connected regions for matrix rearrangement and proposed a cake-cutting (CC order) strategy. The strategy of Xiao *et al.*[7] obtains a new Hadamard by sorting the normal-order Hadamard in the ascending order of the total variation (TV order). Vaz *et al.*[8] compared five sorting methods, among which CC order has the most outstanding performance. Yu *et al.*[9] claimed that the comprehensive performance of the TV order and CC order is better than that of others. Vaz *et al.*[10] presented two new orders, and they have good performance in low-resolution images. Lopez-Garcia *et al.*[11] proposed an order that has at least the same performance and better algorithm complexity than the CC method.

The previous Hadamard sorting methods mentioned above rely on the analysis of the characteristics of each pattern, which is a cumbersome and inefficient process. Pattern selection methods based on Hadamard spectral characteristics have also been raised, in which, however, only just some simple shapes, such as a circle, square, and zigzag were used[12]. In this Letter, we compare the spectral domains of the previous sorting methods and find that the existing orders can be approximated by sampling from low frequency to high frequency. Such sampling paths can reconstruct more reliable images at low sampling rates. However, the absence of the high-frequency components may result in indistinguishable details, blurred edges, and ringing effects. In order to solve the above problems, this Letter proposes a more effective selection method based on spectral domain analysis, which we call the Hadamard SPI sampling strategy based on XY order and probability function (XY + PF). Our method is to obtain the Hadamard spectral energy distribution of the high-frequency and low-frequency information and balance the weights of the two to enhance the image details. This method avoids the complicated process of analyzing each pattern and realizes the overall pattern selection. It has the

advantages of low complexity and high generation speed, and the resolution of important details and edge structures is improved based on a reliable reconstruction of images.

2. Principles and Methods

2.1. SPI with Hadamard basis

As shown in Fig. 1, in the Hadamard SPI, an object is illuminated by a light source, and the reflected light from the object is collected by a lens and imaged on the digital micromirror device (DMD), which is a spatial light modulator. The modulated light is collected by a detector via a lens, which outputs the total light intensity as the measurement value. The above measuring process for Hadamard SPI can be expressed as follows:

$$y = Hx. \tag{1}$$

Here, y is the measurement value, which is the column vector form of total measurements; H is reshaped from the Hadamard pattern loaded on the DMD; and x is the vector form of object. The original image can be obtained by performing the inverse Hadamard transform on the Hadamard spectrum. This Letter adopts the TVAL3[13] algorithm for reconstruction to reduce the reconstruction noise and improve the image quality.

2.2. Hadamard pattern-selection strategy

In the past, most of the Hadamard pattern sorting methods were based on the characteristics of the patterns themselves to determine their position, and researchers rarely cared about its sampling paths on the spectral domain. In this Letter, for the first time, to our knowledge, we compared the spectral domain of the classic and common Hadamard pattern sorting methods (Walsh order, RD order, CC order, TV order). Figure 2 shows the sampling diagrams in the Hadamard spectral domain for six sampling strategies under sampling ratio [SR, $\mathrm{SR} = M/(p \times q)$] of 10%, where $p \times q$ pixels represent the size of the Hadamard spectrum and M is the number of measurements. In the spectral domain sampling diagram, the selected area is white and the unselected area is black. In the Hadamard spectrum, the low-frequency information of the image (object outline and background) is concentrated in the top left corner, while the high-frequency information (object edges and details) is scattered in the bottom right corner. Figure 2 shows that the previous sorting methods are also more inclined to collect the low-frequency information of the image preferentially. However, blindly collecting Hadamard coefficients of low-frequency information will result in the loss of important details of reconstructed images.

Fig. 2. Sampling diagrams in the Hadamard spectral domain for different sampling strategies ($p = q = 256$, SR = 10%).

To improve the speed of sorting patterns and enhance image details, we propose the following strategy: different from the previous methods that analyze the shape of the Hadamard patterns and determine the order, our selection method directly samples the Hadamard spectrum along a direction with better energy concentration and adopts a probability function to balance the weight of different Hadamard spectral components.

Step 1: Sampling paths with high energy concentration are created using coordinate parameter on the Hadamard spectrum. Obtaining Hadamard spectral energy distributions by using image data sets is a common strategy[14–16], and we employ a commonly used image reconstruction dataset DIV2K[17,18]. We performed Hadamard transform on gray-scaled images and then normalized and summed all spectra to obtain the Hadamard power spectrum under this database. The coefficients in the power spectrum are sorted in a descending order to obtain the energy order, which is represented by an index number. The larger the coefficient, the smaller the index number. Therefore, we found the sampling path in which the energy is arranged from large to small on the Hadamard spectrum, as shown in Fig. 3(a).

The method of utilizing a database to obtain sampling paths is deemed to be inefficient, whereas directly sampling a spectrum is a commendable approach for reducing the complexity of pattern generation. To improve the performance, we proposed an XY order to replace the energy order. Through an analysis of the energy order's sampling paths, the XY order is generated by a formula with exceedingly low complexity and retains a certain degree of similarity with the energy order. Additionally, the XY order combines the sampling characteristics of previously well-performed orders (CC order and TV order).

In the XY order, we use the Cartesian coordinates to determine the importance of spectral coefficients and then sort the coefficients and basis patterns accordingly. The generation of the XY order is as follows. (1) Define the upper left corner of the Hadamard spectrum as the coordinate origin, and establish a two-dimensional x–y Cartesian coordinate system. Each spectrum coefficient has its corresponding x and y values. The weight

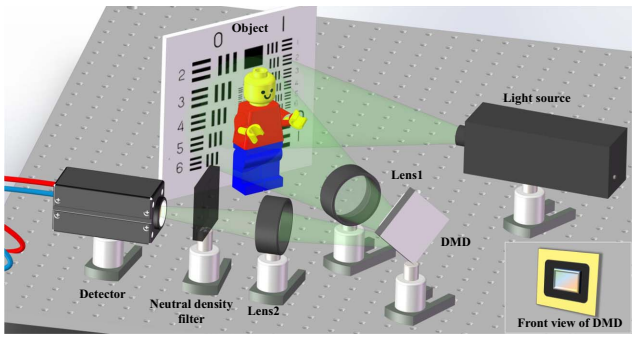

Fig. 1. Schematic of experimental setup.

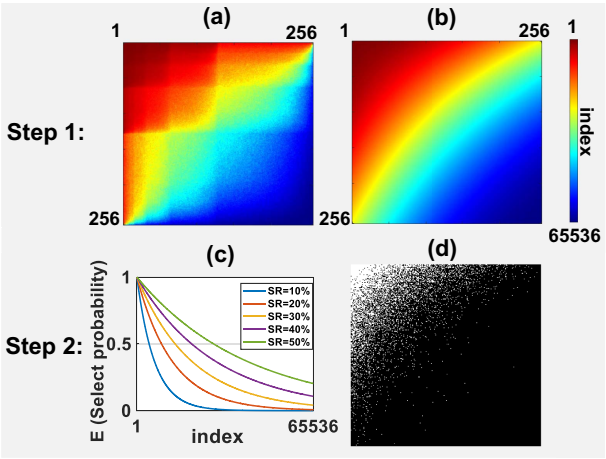

Fig. 3. Hadamard pattern-selection strategy. (a) Sampling path of the energy order, $p = q = 256$; (b) sampling path of the XY order, $p = q = 256$; (c) probability function graph at different SRs; (d) sampling diagram in the Hadamard spectral domain for our method (XY + PF).

value m of each point in the spectrum is calculated according to the following formula:

$$m = x \cdot y + \frac{x^2 + y^2}{4}. \tag{2}$$

(2) Sort the basis patterns in the ascending order of their m values, represented by the index. The patterns with smaller indices are at the front of the XY order. For the basis patterns with the same m value, the order is arbitrary.

The computational complexity of generating Hadamard patterns in different orders has also recently been investigated[11]. Better computational complexity means lower hardware requirements and less generation time. Table 1 shows the generation time required by the three sorting methods for different pattern sizes. The XY order can be generated only by using the spectral coordinates; it does not need to analyze the characteristics of patterns like other orders. Therefore, it has very low complexity and an extremely high generation speed. When generating a Hadamard pattern order of size 256×256, its speed is only 2.7% of the speed of TV order generation. The larger the pattern generated, the more significant the advantage it has on generation speed.

Table 1. Generation Time of Different Hadamard Orders and Different Pattern Sizes (64, 128, and 256).

	Time (s)		
Methods	64	128	256
CC	1.999	23.730	430.785
TV	0.091	1.305	16.659
XY	**0.038**	**0.115**	**0.445**

Step 2: A probability function is used to balance the weights of the different Hadamard spectral components. After obtaining the XY order, a probability function is used to perform random sampling along the direction of energy distribution, i.e., XY order direction to complete the selection of Hadamard patterns at the specified SR. As shown in the Supplementary Material, due to its outstanding performance and computational simplicity in numerous tests, the following probability function has been selected as our method:

$$E(n) = a^{(n-1)/(p \times q)} \qquad (n = 1, \ldots, p \times q), \tag{3}$$

where a $(0 < a < 1)$ is the calculated value obtained using mathematical expectation and summation of the progression, as detailed in the Supplementary Material. When the size of the pattern is determined, the value "a" only varies with the SR, as shown in Fig. 3(c); n is index number of the XY order; and $E(n)$ is the probability that the point number n is selected.

Through the above two steps, sampling diagram in the Hadamard spectral domain for XY + PF method is obtained, as shown in Fig. 3(d); at this time, a is 4.5386×10^{-5} under SR = 10%. The sampling results in the spectral domain demonstrate that our method can perform proportional sampling of both the high- and low-frequency components of the spectrum. As each pattern corresponds to a point in the Hadamard domain, the selection of the desired pattern is accomplished upon obtaining the sampling diagram. The image reconstruction can be achieved by modulating these Hadamard patterns according to the method described in Section 2.1.

3. Simulation Results

Two classic images were chosen: the USAF1951 resolution target and a camera man. Both of them have a resolution of 256×256 pixels and mixed 1% Gaussian noise to simulate the real situation.

The resolution target simulation results obtained using the XY + PF sampling strategy have complete structures and good quantization value—better than those of other orders, as shown in Fig. S2 in the Supplementary Material. Two detail regions are selected to demonstrate that our method can improve the detail of the reconstructed image. Figure 4(a) shows that the stripe part (red square) and number part (yellow square) in the image are selected for comparison experiments. In Figs. 4(b) and 4(c), for the stripe part, Walsh order and RD order all have parts that cannot be reconstructed successfully. The CC order has excellent resolution for striped objects, but the stripe edges are still a little blurry. The TV order did not have sufficient reconstruction ability for the thinnest fringes. Our method (XY + PF) recovered the sharpest stripes under the same SR. For the number part, it is obvious that the number of XY + PF is fine and the resolution is the highest. Figures 4(d) and 4(e) show the results of the quantitative analysis of the detail part. Each point shows the mean

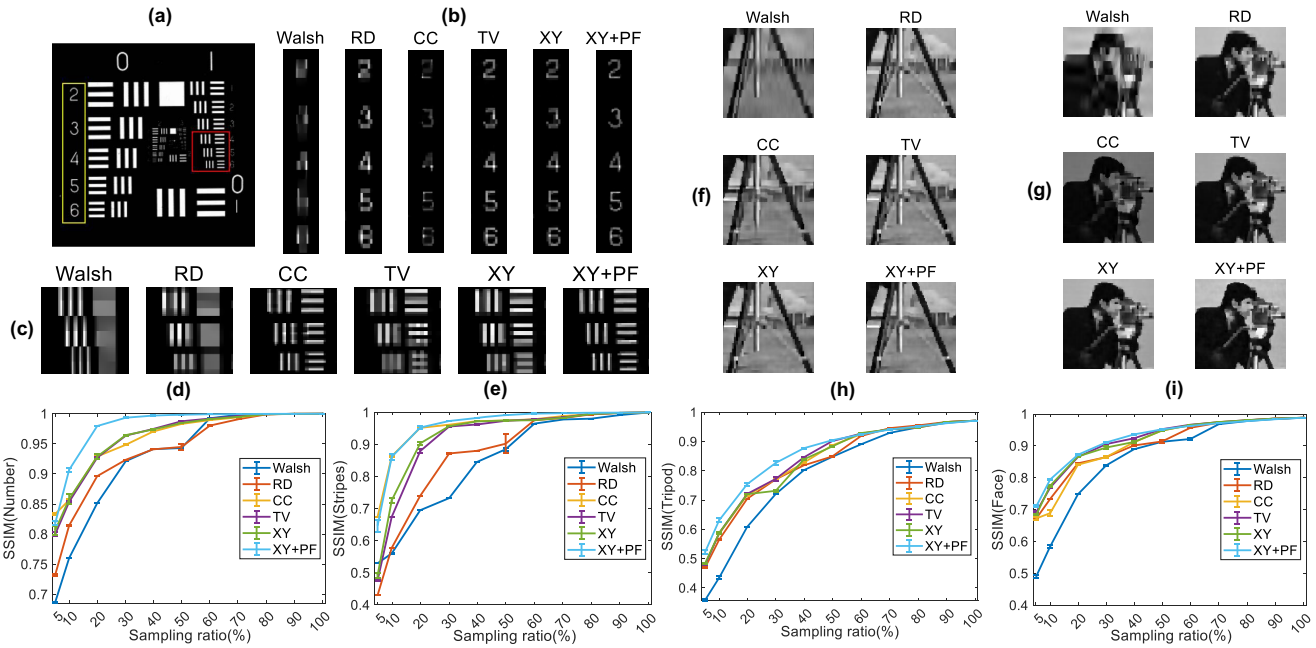

Fig. 4. Detailed reconstruction results of the resolution target and camera man. (a) Two selected detailed areas of the resolution target; (b) closeups of the number part (SR = 10%); (d) shows the SSIMs in the (b) area. (c) Closeups of the stripe part (SR = 10%); (e) shows the SSIMs in the (c) area. (f) Closeups of the tripod part (SR = 10%); (h) shows the SSIMs in the (f) area. (g) Closeups of the face part (SR = 10%); (i) shows the SSIMs in the (g) area.

values of five measurements with added noise. Error bars have been added to all quantified data, and the height of the error bars indicates the standard deviation. The SSIM values of XY + PF in the striped part is similar to that of the CC order, but it has much stronger performance than the other orders in the number part.

A gray-scale image camera man was used for further testing. Figure S3 in the Supplementary Material shows the effect of six methods in recovering the overall information and the quantitative results. For detailed reconstruction performance, Fig. 4 shows the comparison closeups of the details. As shown in Fig. 4(f), for the "tripod" part, our method (XY + PF) can better outline the boundary contour of the main object and make the main object stand out from the background. For the "face" part in Fig. 4(g), the facial features of the reconstructed image obtained under the same conditions using our method are more prominent and clear. The ringing effect at the border of the hair and coat is suppressed, the jagged streaks of the hand-holding pole are reduced, and the detailed resolution is improved. Compared with other methods, our method has significantly improved the quantization values except for Fig. 4(i), which we attribute to the presence of a large amount of low-frequency information in this region. The line graphs of SSIM in Figs. 4(h) and 4(i) demonstrate the above analysis well.

4. Experimental Results

To demonstrate the feasibility of our sampling strategy, an actual experiment was conducted. In our experimental setup (see Fig. 1), the light source was an LED parallel light (KM-SPP505-W). The loaded Hadamard pattern size was 128 × 128 pixels, and the DMD (TI DLP7000) ran at a frame rate of 30 Hz, which is the upper limit of the detector's frame rate. The detector in this Letter was a charge-coupled device (CCD, IMPERX B1620M), which was used as a bucket detector without spatial resolution[19–21]. In this experiment, the target object was a toy figurine, and its background was the standard USAF1951 resolution target. The reconstructed image obtained at SR = 100% was used as the original image.

Our method reconstructed the gray-scale object (toy sculptures in the Supplementary Material) well (see Fig. S4), and paid attention to the details of the resolution version in the background. The selected areas in the red box correspond to Group 0 on the USAF1951 target [see Fig. 5(a)]. Figure 5(b) quantitatively demonstrates the superiority of the proposed sampling strategy. The reconstructed closeups and extracted intensity profiles of the cross section red and blue lines are depicted in Fig. 5(c). As shown in these closeups, the XY order exhibited a similar reconstruction performance compared to the best of previous orders, and the proposed XY + PF strategy completely recovered the stripes with details, outperforming the other sampling methods. Meanwhile, the greater undulation of the intensity profile means finer details. From the point of view of the intensity profiles, the proposed XY + PF method correctly distinguished three horizontal and vertical stripes with high resolution; meanwhile, the remaining orders can identify two stripes at most. These figures demonstrate that the proposed

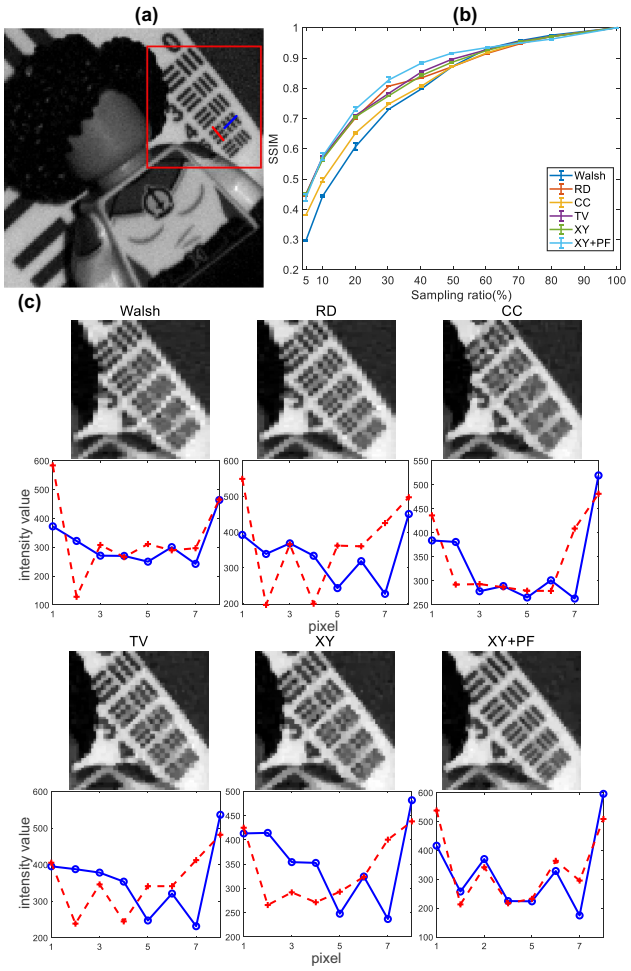

Fig. 5. Detailed experimental reconstruction results. (a) Selected detailed area of the target object; (b) SSIMs in detailed area; (c) closeups of details (SR = 40%) and intensity profiles of the cross section red and blue lines depicted in (a).

XY + PF method can improve the detailed resolution based on a better reconstruction of the entire target.

5. Conclusion

We propose a detail-enhanced Hadamard basis sampling strategy based on XY order and probability function (XY + PF). The XY order exhibits good performance and an extremely short generation time, generating a Hadamard pattern order of size 256×256 in only 0.445 s. Then, an exponential function is used as the probability function to sample the XY order to obtain the required Hadamard patterns. The simulation and experimental results show that the imaging quality of the XY + PF sampling strategy can increase the resolution of important details, suppress the ringing effect, and highlight edge information. It may be essential to study the characteristics of Hadamard spectral energy distribution, which has potential applications in adaptively selecting the proportion of high-frequency or low-frequency information in a reconstructed image.

Acknowledgement

This work was supported by the Beijing Institute of Technology Research Fund Program for Young Scholars (No. 202122012).

References

1. G. M. Gibson, S. D. Johnson, and M. J. Padgett, "Single-pixel imaging 12 years on: a review," Opt. Express **28**, 28190 (2020).
2. M. F. Duarte, M. A. Davenport, D. Takhar, J. N. Laska, T. Sun, K. F. Kelly, and R. G. Baraniuk, "Single-pixel imaging via compressive sampling," IEEE Signal Process. Mag. **25**, 83 (2008).
3. E. J. Candes and M. B. Wakin, "An introduction to compressive sampling," IEEE Signal Process. Mag. **25**, 21 (2008).
4. Z. Cai, H. Zhao, M. Jia, G. Wang, and J. Shen, "An improved Hadamard measurement matrix based on Walsh code for compressive sensing," in *9th International Conference on Information, Communications and Signal Processing* (2013), p. 1.
5. M.-J. Sun, M. Tong, M. Edgar, M. Padgett, and N. Radwell, "A Russian Dolls ordering of the Hadamard basis for compressive single-pixel imaging," Sci. Rep. **7**, 3464 (2017).
6. W.-K. Yu, "Super sub-Nyquist single-pixel imaging by means of cake-cutting Hadamard basis sort," Sensors **19**, 4122 (2019).
7. X. Yu, R. Stantchev, F. Yang, and E. Pickwell-MacPherson, "Super sub-Nyquist single-pixel imaging by total variation ascending ordering of the Hadamard basis," Sci. Rep. **10**, 9338 (2020).
8. P. G. Vaz, D. Amaral, L. F. R. Ferreira, M. Morgado, and J. Cardoso, "Image quality of compressive single-pixel imaging using different Hadamard orderings," Opt. Express **28**, 11666 (2020).
9. X. Yu, F. Yang, B. Gao, J. Ran, and X. Huang, "Deep compressive single pixel imaging by reordering Hadamard basis: a comparative study," IEEE Access **8**, 55773 (2020).
10. P. Vaz, A. Gaudêncio, L. Ferreira, A. Humeau-Heurtier, M. Morgado, and J. Cardoso, "Re-ordering of Hadamard matrix using Fourier transform and gray-level co-occurrence matrix for compressive single-pixel imaging in low resolution images," IEEE Access **10**, 46975 (2022).
11. L. López-García, W. Cruz-Santos, A. García-Arellano, P. Filio-Aguilar, J. A. Cisneros-Martínez, and R. Ramos-García, "Efficient ordering of the Hadamard basis for single pixel imaging," Opt. Express **30**, 13714 (2022).
12. Z. Zhang, X. Wang, G. Zheng, and J. Zhong, "Hadamard single-pixel imaging versus Fourier single-pixel imaging," Opt. Express **25**, 19619 (2017).
13. C. Li, *An Efficient Algorithm for Total Variation Regularization with Applications to the Single Pixel Camera and Compressive Sensing* (Rice University, 2011).
14. C. Higham, R. Murray-Smith, M. Padgett, and M. Edgar, "Deep learning for real-time single-pixel video," Sci. Rep. **8**, 2369 (2018).
15. K. Czajkowski, A. Pastuszczak, and R. Kotyński, "Real-time single-pixel video imaging with Fourier domain regularization," Opt. Express **26**, 20009 (2018).
16. A. Y. Yuan, J. Feng, S. Jiao, Y. Gao, Z. Zhang, Z. Xie, L. Du, and T. Lei, "Adaptive and dynamic ordering of illumination patterns with an image dictionary in single-pixel imaging," Opt. Commun. **481**, 126527 (2021).
17. R. Timofte, S. Gu, J. Wu, L. Van Gool, L. Zhang, M.-H. Yang, M. Haris, G. Shakhnarovich, N. Ukita, S. Hu, Y. Bei, Z. Hui, X. Jiang, Y. Gu, J. Liu, Y. Wang, F. Perazzi, B. McWilliams, A. Sorkine-Hornung, O. Sorkine-Hornung, C. Schroers, J. Yu, Y. Fan, J. Yang, N. Xu, Z. Wang, X. Wang, T. S. Huang, X. Wang, K. Yu, T.-W. Hui, C. Dong, L. Lin, C. C. Loy, D. Park, K. Kim, S. Y. Chun, K. Zhang, P. Liu, W. Zuo, S. Guo, J. Liu, J. Xu, Y. Liu, F. Xiong, Y. Dong, H. Bai, A. Damian, N. Ravi, S. Menon, C. Rudin, J. Seo, T. Jeon, J. Koo, S. Jeon, S. Y. Kim, J.-S. Choi, S. Ki, S. Seo, H. Sim, S. Kim, M. Kim, R. Chen, K. Zeng, J. Guo, Y. Qu, C. Li, N. Ahn, B. Kang, K.-A. Sohn, Y. Yuan, J. Zhang, J. Pang, X. Xu, Y. Zhao, W. Deng, S. Ul Hussain, M. Aadil, R. Rahim, X. Cai, F. Huang, Y. Xu, P. N. Michelini, D. Zhu, H. Liu, J.-H. Kim, J.-S. Lee, Y. Huang, M. Qiu,

L. Jing, J. Zeng, Y. Wang, M. Sharma, R. Mukhopadhyay, A. Upadhyay, S. Koundinya, A. Shukla, S. Chaudhury, Z. Zhang, Y. H. Hu, and L. Fu, "Ntire 2018 challenge on single image super-resolution: methods and results," in *IEEE/CVF Conference on Computer Vision and Pattern Recognition Workshops (CVPRW)* (2018), p. 965.
18. Z. Qiu, X. Guo, T. Lu, P. Qi, Z. Zhang, and J. Zhong, "Efficient Fourier single-pixel imaging with Gaussian random sampling," Photonics **8**, 319 (2021).
19. F. Ferri, D. Magatti, A. Gatti, M. Bache, E. Brambilla, and L. A. Lugiato, "High-resolution ghost image and ghost diffraction experiments with thermal light," Phys. Rev. A **94**, 183602 (2005).
20. L. Zhou, X. Huang, Q. Fu, X. Zou, Y. Bai, and X. Fu, "Fine edge detection in single-pixel imaging," Chin. Opt. Lett. **19**, 121101 (2021).
21. X. Nie, X. Zhao, T. Peng, and M. O. Scully, "Sub-Nyquist computational ghost imaging with orthonormal spectrum-encoded speckle patterns," Phys. Rev. A **105**, 043525 (2022).